A Unified Gram-Schmidt–Ritz Solution for Vibration Analysis of Nanoplates with Elastic Boundary Conditions

Hossein Pakdaman

Department of Civil Engineering, K.N. Toosi University of Technology, Valiasr Ave., Tehran, Iran
Email(s): Hosseinpakdaman@email.kntu.ac.ir

Abstract:

A novel and unified approach is presented for analyzing the free vibration of rectangular nanoplates with elastic boundary conditions. The theoretical modeling is achieved using the nonlocal Mindlin plate theory, which accounts for the size-dependent behavior of nanoplates, while the artificial spring technique is employed to accommodate a wide range of boundary conditions, including classical boundary conditions, elastic boundary conditions, and their combinations. The governing equations of motion are derived using the virtual displacement principle, followed by the application of the weighted residual method to obtain the nonlocal quadratic functional. The Rayleigh-Ritz method, employing Gram-Schmidt polynomial series as the admissible displacement functions, is then utilized to solve the eigenvalue problems associated with the free vibration of nanoplates. The present approach is validated through a series of comparison and convergence studies, which demonstrate its high accuracy and low computational cost. Finally, parametric numerical investigations are conducted to elucidate the effects of variations in spring stiffness on the natural frequencies of nanoplates. It is shown that the proposed method can easily compute the natural frequencies of nanoplates with elastic boundary conditions.

Keywords:

Free vibration, Nanoplate, Gram-Schmidt polynomial, Rayleigh–Ritz method, Elastic boundary conditions.

1. Introduction

Nano-scale plates, such as graphene sheets, boron-nitride sheets, gold nanoplates, and silver nanoplates, have unlocked a wealth of promising applications in nanoscience and nanotechnology [1,2]. These intriguing applications include, but are not limited to, bio and mechanical sensors [3], supercapacitors and energy storage systems [4], anti-corrosion coatings [5], electrocatalysts [6] as well as lithium-ion batteries [7]. In most of the above-mentioned applications, the precise prediction of the vibrational behavior of nanoplates plays a pivotal role since the performance and effectiveness of these nano-scale systems are inextricably linked to their mechanical characteristics such as natural frequencies.

Among numerous continuum theories, including strain gradient theory [8-10], nonlocal elasticity theory [11-13], couple stress elasticity theory [14-17] and micromorphic theory [18], Eringen's nonlocal theory of elasticity has emerged as the most widely used theory for addressing the size effects. This theory is based on the idea that a continuous system is highly interconnected. To address the size-dependent effects and incorporate atomic interactions into traditional continuum-based theories, a nonlocal factor is introduced in this theory. Peddieson et al. [19] pioneered the application of nonlocal elasticity theory to investigate the nonlocality effects on the bending behavior of Euler–Bernoulli nanobeams. Thereafter, this theory has been widely employed to analyze the linear and nonlinear bending, buckling and vibration behavior of different nano-scale structures, such as nanobeams [20-22], nanoplates [23,24], nanorods [25,26] and nanowires [27, 28].

The free vibration analysis of nanoplates with general boundary conditions (BCs) has received relatively less attention compared to one-dimensional nanostructures. However, there are a few studies that have provided important findings in this field. In this regard, Lu et al. [29] proposed exact nonlocal solutions for the bending and free vibration of the nanoplate with simply supported BCs, using the nonlocal Kirchhoff plate (NKP) and nonlocal Mindlin plate (NMP). Afterward, numerous numerical and analytical techniques were employed for the nonlocal buckling and vibration analyses of nanoplates. The most commonly used numerical methodologies include the Finite element method [30,31], the Galerkin method [32], the differential quadrature method [33,34], the Rayleigh-Ritz method [35], the finite strip method [36,37], the Chebyshev collocation method [38], the element-free kp-Ritz method [39] and the discrete singular convolution method [40].

Exact analytical solutions also exist for rectangular nanoplates having at least two parallel simply supported BCs. Using the Navier method, researchers have achieved exact solutions for bending, buckling and vibration responses of simply-supported nanoplates based on various plate models, including the NKP [41], NMP [42], second-order shear deformation model [43], and higher-order plate models [44]. Similarly, exact buckling and vibration solutions for nanoplates with Levy-type BCs have been obtained using the

NKP [45,46], NMP [47], and higher-order plate models [48]. Furthermore, studies have been conducted on nanoplates with non-Levy BCs based on the NKP. Zheng et al. [49] utilized the symplectic superposition approach to derive series-based analytic solutions for bending and vibration of nanoplates with a combination of clamped/simply-supported BCs. Additionally, Wang et al. [50] presented an iterative approach based on the separation-of-variable approach to examine the free vibration of nanoplates with general homogeneous BCs.

In the aforementioned studies concerning the vibration of nanoplates, only classical BCs, namely simply supported, clamped, or free BCs, along with their combinations, were taken into account. However, classical BCs may not always apply in practical engineering as some unknown elastic constraints may appear in the actual situation [51]. Under such conditions, relying only on classical BCs may lead to significant errors and inaccuracies in engineering analyses. Hence, the development of a unified and efficient formulation capable of addressing nanoplates with general BCs is critical and of paramount significance. In the simulation of general boundaries, one of the widely used methods is the artificial spring technique, which involves the implementation of distributed artificial springs with suitable stiffness along all edges of the nanoplates. Subsequently, the Rayleigh-Ritz method is adopted, and appropriate sets of admissible functions such as the modified Fourier series [52], Chebyshev polynomials [53], and Gram-Schmidt polynomials [54] are chosen to develop a unified solution. Researchers have analyzed the accuracy, rate of convergence, and computational efficiency of these three distinct sets of admissible functions. Their findings reveal that Chebyshev polynomials and Gram-Schmidt polynomials outperform the modified Fourier series substantially in both convergence speed and computational efficiency [55]. Furthermore, among these functions, Gram-Schmidt polynomials offer several advantages, such as improved matrix conditioning, increased numerical stability, and minimized susceptibility to round-off errors. Their efficient computation through recurrence relations also enhances overall performance, making them particularly effective for problems with elastic BCs. Although the artificial spring method has been utilized for the vibration of classical plates [56-58], its application to nonlocal nanoplates has not yet been reported.

To the best of the author's knowledge, this study is the first to investigate the vibrations of rectangular nanoplates with general elastic BCs using nonlocal elasticity theory, capturing size-dependent effects under arbitrary BCs. In the context of NMP theory, the direct formulation of the potential energy functional based on constitutive relations is not straightforward. Therefore, this paper introduces the weak forms of the equations of motion employing the weighted residual method (WRM) to obtain the nonlocal quadratic functional. Furthermore, the displacement components are expanded by the Gram-Schmidt polynomials. By combining these expansions with the nonlocal quadratic functional and employing the Rayleigh-Ritz

procedure, a standard eigenproblem is developed. The convergence of the proposed method is verified, and its accuracy is validated through comparative analysis of the obtained results against those previously reported by other researchers in the field. Parametric studies are also conducted to examine the free vibration behavior of nanoplates under different classical BCs and elastic restraints BCs as well as their combinations.

1. Theoretical formulations

1.1. Nanoplate model description

Consider a rectangular nanoplate with length *a*, width *b* and thickness *h*, as illustrated in Fig 1. Assigning coordinates *x*, *y*, and *z* to align with the longitudinal, width, and transverse directions, respectively, a Cartesian coordinate system (*x*, *y*, *z*) is introduced and fixed on the middle surface of the nanoplate. Within this frame of reference, the component of the deformation of the nanoplate is denoted by *w* in the transverse direction. The material properties of the nanoplate are isotropic with Young's modulus *E*, shear modulus *G*, mass density ρ, and Poisson's ratio ν. Along each end of nanoplate, a group of translational springs with stiffness k_w and two groups of rotational springs with stiffnesses k_x and k_y are introduced to simulate the classical and non-classical BCs. The desired BCs can be readily achieved by properly assigning the springs with appropriate stiffness values. For instance, a clamped BC can be constructed by setting the stiffness values of all the springs to an extremely high value.

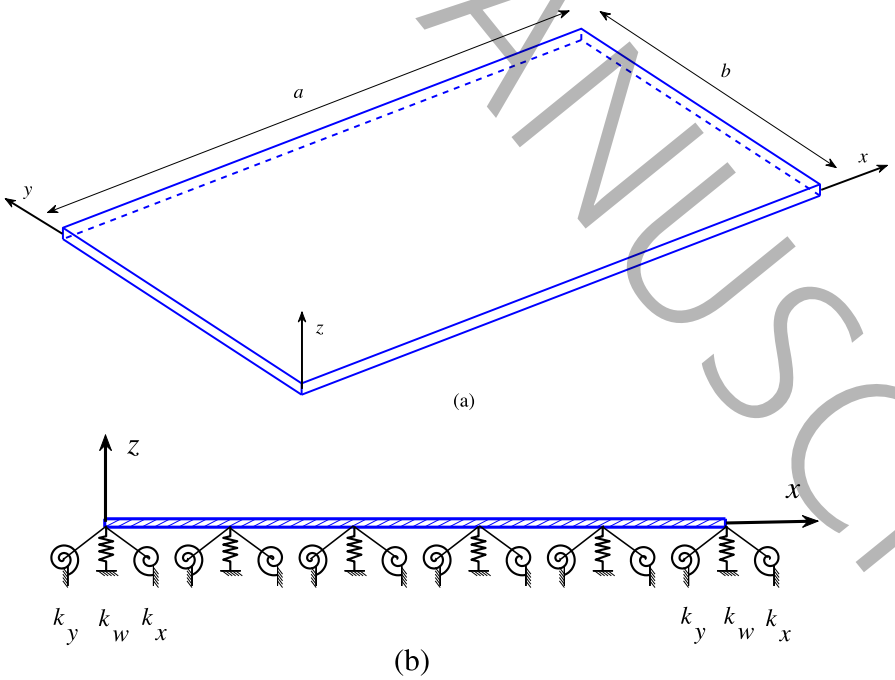

Fig. 1. Schematic plot of a nanoplate: (a) geometry and coordinates, (b) side view with boundary springs.

1.2. Mindlin plate model

Based on NMP theory, the strain components (ε_{ij}) are given by [59]:

$$\epsilon_{xx} = -z\frac{\partial \psi_x}{\partial x}, \quad \epsilon_{yy} = -z\frac{\partial \psi_y}{\partial y}, \quad \epsilon_{zz} = 0, \quad \gamma_{xz} = \frac{\partial w}{\partial x} - \psi_x, \quad \gamma_{yz} = \frac{\partial w}{\partial y} - \psi_y, \quad \gamma_{xy} = -z\left(\frac{\partial \psi_x}{\partial y} + \frac{\partial \psi_y}{\partial x}\right), \tag{1}$$

where ψ_x and ψ_y denote the rotation angles of the *x*-*z* and *y*-*z* planes, respectively. Based on the nonlocal theory, the differential constitutive relation is expressed as $\left(1-l_s^2\nabla^2\right)\sigma^{nl} = \sigma^l$ in which σ^{nl} and σ^l represent the nonlocal stress and local stress, respectively, l_s is the nonlocal factor and ∇^2 denotes the Laplacian operator and is given by $\nabla^2(.) = \partial^2(.)/\partial x^2 + \partial^2(.)/\partial y^2$ for a two-dimensional space. The nonlocal factor, $l_s = e_0 l$, is defined by the coupling of a material constant e_0, which is determined through experimental methods or atomistic dynamics for each specific material, along with an internal characteristic length *l*, which relates to molecular distances, the lattice parameter, and granular size [60].

Taking into account Hooke's law and differential model of nonlocal theory, the constitutive equations for the nanoplate can be formulated as follows [59]:

$$(1-l_s^2\nabla^2)\sigma_{xx}^{nl} = \frac{E}{1-\nu^2}(\epsilon_{xx} + \nu\epsilon_{yy}), \quad (1-l_s^2\nabla^2)\sigma_{yy}^{nl} = \frac{E}{1-\nu^2}(\epsilon_{yy} + \nu\epsilon_{xx}), \quad (1-l_s^2\nabla^2)\tau_{xy}^{nl} = G\gamma_{xy}, \tag{2a}$$

$$(1-l_s^2\nabla^2)\tau_{xz}^{nl} = G\gamma_{xz}, \quad (1-l_s^2\nabla^2)\tau_{yz}^{nl} = G\gamma_{yz}, \tag{2b}$$

By multiplying both sides of Eq. (2a) by *z*, considering Eq. (1), and integrating over the thickness, we obtain the nonlocal moment stress resultants as [59]:

$$(1-l_s^2\nabla^2)M_{xx}^{nl} = D\left(\frac{\partial \psi_x}{\partial x} + \nu\frac{\partial \psi_y}{\partial y}\right), \tag{3a}$$

$$(1-l_s^2\nabla^2)M_{yy}^{nl} = D\left(\frac{\partial \psi_y}{\partial y} + \nu\frac{\partial \psi_x}{\partial x}\right), \tag{3b}$$

$$(1-l_s^2\nabla^2)M_{xy}^{nl} = D\frac{(1-\nu)}{2}\left(\frac{\partial \psi_x}{\partial y} + \frac{\partial \psi_y}{\partial x}\right), \tag{3c}$$

where $D = Eh^3 / \left[12\left(1-\nu^2\right)\right]$ is the flexural rigidity. Similarly, the nonlocal shear force resultants can be obtained by integrating both sides of Eq. (2b) over the thickness, i.e.,

$$(1-l_s^2\nabla^2)Q_x^{nl} = S\left(\psi_x + \frac{\partial w}{\partial x}\right), \quad (1-l_s^2\nabla^2)Q_y^{nl} = S\left(\psi_y + \frac{\partial w}{\partial y}\right), \tag{4}$$

where $S = k_s Gh$ and k_s denote the shear correction factor. To derive the differential equations of motion in terms of w, ψ_x and ψ_y, the virtual displacement principle is used together with Eqs. (3a)-(3c) and (4), which leads to the following governing equations and BCs for the nanoplate:

$$S\left(\frac{\partial^2 w}{\partial x^2} + \frac{\partial^2 w}{\partial y^2} - \frac{\partial \psi_x}{\partial x} - \frac{\partial \psi_y}{\partial y}\right) = (1-l_s^2\nabla^2)\left[I_0 \frac{\partial^2 w}{\partial t^2}\right], \tag{5a}$$

$$D\left(\frac{\partial^2 \psi_x}{\partial x^2} + \frac{(1+\nu)}{2}\frac{\partial^2 \psi_y}{\partial x \partial y} + \frac{(1-\nu)}{2}\frac{\partial^2 \psi_x}{\partial y^2}\right) + S\left(\frac{\partial w}{\partial x} - \psi_x\right) = (1-l_s^2\nabla^2)\left[I_2 \frac{\partial^2 \psi_x}{\partial t^2}\right], \tag{5b}$$

$$D\left(\frac{\partial^2 \psi_y}{\partial y^2} + \frac{(1+\nu)}{2}\frac{\partial^2 \psi_x}{\partial x \partial y} + \frac{(1-\nu)}{2}\frac{\partial^2 \psi_y}{\partial x^2}\right) + S\left(\frac{\partial w}{\partial y} - \psi_y\right) = (1-l_s^2\nabla^2)\left[I_2 \frac{\partial^2 \psi_y}{\partial t^2}\right], \tag{5c}$$

and

$$k_w^{x0} w = -Q_x^{nl}, \quad k_x^{x0}\psi_x = -M_{xx}^{nl}, \quad k_y^{x0}\psi_y = -M_{xy}^{nl} \quad \text{at } x = 0, \tag{6a}$$

$$k_w^{xa} w = Q_x^{nl}, \quad k_x^{xa}\psi_x = M_{xx}^{nl}, \quad k_y^{xa}\psi_y = M_{xy}^{nl} \quad \text{at } x = a, \tag{6b}$$

$$k_w^{y0} w = -Q_y^{nl}, \quad k_y^{y0}\psi_y = -M_{yy}^{nl}, \quad k_x^{y0}\psi_x = -M_{xy}^{nl} \quad \text{at } y = 0, \tag{6c}$$

$$k_w^{yb} w = Q_y^{nl}, \quad k_y^{yb}\psi_y = M_{yy}^{nl}, \quad k_x^{yb}\psi_x = M_{xy}^{nl} \quad \text{at } y = b, \tag{6d}$$

where $I_0 = \rho h$, $I_2 = \rho h^3/12$, k_w^{x0}/k_w^{xa}, k_x^{x0}/k_x^{xa} and k_y^{x0}/k_y^{xa} are the springs' stiffness at the edge $x = 0/x = a$ and k_w^{y0}/k_w^{yb}, k_x^{y0}/k_x^{yb} and k_y^{y0}/k_y^{yb} are the springs' stiffness at the edge $y = 0/y = b$. The derived nonlocal differential equations can easily be reduced to the classical ones by setting $l_s = 0$.

Assuming modal motion, we express the displacement and rotation fields as: $w(x,y,t) = w^*(x,y)e^{i\omega t}$, $\psi_x(x,y,t) = \psi_x{}^*(x,y)e^{i\omega t}$ and $\psi_y(x,y,t) = \psi_y{}^*(x,y)e^{i\omega t}$, where ω is the natural frequency. For convenience and simplification, we introduce the following dimensionless quantities, dropping the subscripts * for simplicity:

$$\bar{w}=\frac{w}{a},\xi=\frac{x}{a},\eta=\frac{y}{b},\ \bar{\psi}_{\xi}=\psi_x,\bar{\psi}_{\eta}=\psi_y,\bar{\omega}=\omega a\sqrt{\frac{I_0}{S}},\gamma=\frac{a}{b},\kappa=\frac{h}{a},\ \bar{l}_s=\frac{l_s}{a},\bar{I}_2=\frac{I_2}{I_0a^2},$$

$$\bar{D}=\frac{\kappa^2}{6k_s(1-\nu)},\ \bar{\nabla}^2(\cdot)=\frac{\partial^2(\cdot)}{\partial\xi^2}+\gamma^2\frac{\partial^2(\cdot)}{\partial\eta^2},\bar{k}_w^{[n]}=\frac{k_w^{[.]}a^2}{S},\bar{k}_x^{[n]}=\frac{k_x^{[.]}}{S},\bar{k}_y^{[n]}=\frac{k_y^{[.]}}{S},$$

$$[.]=x_0,x_a,y_0,y_b;\ \ [\mathrm{n}]=\xi_0,\xi_1,\eta_0,\eta_1, \tag{7}$$

Using Eqs. (5a)-(5c) and (7), the nonlocal dimensionless equations for the vibration analysis of nanoplates are obtained as:

$$(1-\bar{l}_s^2\bar{\nabla}^2)[\bar{\omega}^2\bar{w}]+\left(\frac{\partial^2\bar{w}}{\partial\xi^2}+\gamma^2\frac{\partial^2\bar{w}}{\partial\eta^2}-\frac{\partial\bar{\psi}_{\xi}}{\partial\xi}-\gamma\frac{\partial\bar{\psi}_{\eta}}{\partial\eta}\right)=0, \tag{8a}$$

$$(1-\bar{l}_s^2\bar{\nabla}^2)[\bar{\omega}^2\bar{I}_2\bar{\psi}_{\xi}]+\bar{D}\left(\frac{\partial^2\bar{\psi}_{\xi}}{\partial\xi^2}+\frac{(1+\nu)}{2}\gamma\frac{\partial^2\bar{\psi}_{\eta}}{\partial\xi\partial\eta}+\frac{(1-\nu)}{2}\gamma^2\frac{\partial^2\bar{\psi}_{\xi}}{\partial\eta^2}\right)+\left(\frac{\partial\bar{w}}{\partial\xi}-\bar{\psi}_{\xi}\right)=0, \tag{8b}$$

$$(1-\bar{l}_s^2\bar{\nabla}^2)[\bar{\omega}^2\bar{I}_2\bar{\psi}_{\eta}]+\bar{D}\left(\gamma^2\frac{\partial^2\bar{\psi}_{\eta}}{\partial\eta^2}+\frac{(1+\nu)}{2}\gamma\frac{\partial^2\bar{\psi}_{\xi}}{\partial\xi\partial\eta}+\frac{(1-\nu)}{2}\frac{\partial^2\bar{\psi}_{\eta}}{\partial\xi^2}\right)+\left(\gamma\frac{\partial\bar{w}}{\partial\eta}-\bar{\psi}_{\eta}\right)=0, \tag{8c}$$

2. Solution methodology

In this section, the energy-oriented Rayleigh–Ritz method is applied to examine the vibration behavior of nanoplates. This approach involves formulating a quadratic functional whose minimization yields a solution that matches the governing equation. Classical elasticity theory utilizes the principle of minimum total potential energy to construct the minimization functional. This principle assumes that the stress at a given location can be uniquely determined from the strain at that same point [61]. In contrast, the nonlocal elasticity theory reveals that the stress at a generic point depends on the stresses within the surrounding neighborhood, not just the local strain. As a result, an inverse method is employed here to derive the quadratic form of the total potential energy directly from the governing equations, rather than relying on the minimum potential energy principle. This inverse approach starts with the governing equations and works backwards to obtain the desired quadratic functional form, which can then be minimized to determine the vibration solution.

2.1. Weak formulation

The partial differential equations expressed in Eqs. (8a)-(8c) represent the strong form of the equations of motion for the vibration analysis of nanoplates. In order to establish a weak form of the system of equations, one can employ the energy principle or WRM. The WRM is a more general mathematical

technique that can be used to approximately solve a wide range of partial differential equations. Based on this method, the weak form of equations of motion, given by Eqs. (8a)-(8c), is expressed as follows:

$$\iint_S \left\{ \begin{array}{l} \left[(1-\bar{l}_s^{\,2}\bar{\nabla}^2)\left(\bar{\omega}^2\bar{w} + \bar{P}\left(\frac{\partial^2\bar{w}}{\partial\xi^2} + \gamma^2\frac{\partial^2\bar{w}}{\partial\eta^2} \right) \right) + \left(\frac{\partial^2\bar{w}}{\partial\xi^2} + \gamma^2\frac{\partial^2\bar{w}}{\partial\eta^2} - \frac{\partial\bar{\psi}_\xi}{\partial\xi} - \gamma\frac{\partial\bar{\psi}_\eta}{\partial\eta} \right)\delta\bar{w} \right] \\ + \left[(1-\bar{l}_s^{\,2}\bar{\nabla}^2)\left(\bar{\omega}^2\bar{I}_2\bar{\psi}_\xi \right) + \bar{D}\left(\frac{\partial^2\bar{\psi}_\xi}{\partial\xi^2} + \frac{(1+\nu)}{2}\gamma\frac{\partial^2\bar{\psi}_\eta}{\partial\xi\partial\eta} + \frac{(1-\nu)}{2}\gamma^2\frac{\partial^2\bar{\psi}_\xi}{\partial\eta^2} \right) \right]\delta\bar{\psi}_\xi \\ + \left[(1-\bar{l}_s^{\,2}\bar{\nabla}^2)\left(\bar{\omega}^2\bar{I}_2\bar{\psi}_\eta \right) + \bar{D}\left(\gamma^2\frac{\partial^2\bar{\psi}_\eta}{\partial\eta^2} + \frac{(1+\nu)}{2}\gamma\frac{\partial^2\bar{\psi}_\xi}{\partial\xi\partial\eta} + \frac{(1-\nu)}{2}\frac{\partial^2\bar{\psi}_\eta}{\partial\xi^2} \right) \right]\delta\bar{\psi}_\eta \\ + \left(\gamma\frac{\partial\bar{w}}{\partial\eta} - \bar{\psi}_\eta \right)\delta\bar{\psi}_\eta + \left(\frac{\partial\bar{w}}{\partial\xi} - \bar{\psi}_\xi \right)\delta\bar{\psi}_\xi \end{array} \right\} d\xi d\eta = 0, \quad (9)$$

where S represents the nanoplate domain. By applying integration by parts to Eq. (9), disregarding the boundary terms and incorporating potential energies stored in the springs, the following quadratic functional for the nanoplate is derived:

$$\Pi(\xi,\eta) = U(\xi,\eta) + U_{sp}(\xi,\eta) - \bar{\omega}^2 T(\xi,\eta), \quad (10)$$

in which

$$U(\xi,\eta) = \frac{1}{2}\int_0^1\int_0^1 \left\{ \begin{array}{l} \bar{D}\left[\left(\frac{\partial\bar{\psi}_\xi}{\partial\xi} \right)^2 + 2\nu\gamma\frac{\partial\bar{\psi}_\xi}{\partial\xi}\frac{\partial\bar{\psi}_\eta}{\partial\eta} + \gamma^2\left(\frac{\partial\bar{\psi}_\eta}{\partial\eta} \right)^2 \right] + \\ \frac{(1-\nu)\bar{D}}{2}\left(\gamma\frac{\partial\bar{\psi}_\xi}{\partial\eta} + \frac{\partial\bar{\psi}_\eta}{\partial\xi} \right)^2 + \left(\frac{\partial\bar{w}}{\partial\xi} - \bar{\psi}_\xi \right)^2 + \left(\gamma\frac{\partial\bar{w}}{\partial\eta} - \bar{\psi}_\eta \right)^2 \end{array} \right\} d\xi d\eta, \quad (11a)$$

$$\begin{array}{l} U_{sp}(\xi,\eta) = \frac{1}{2}\int_0^1 \left[\bar{k}_w^{\xi 0}\bar{w}^2 + \bar{k}_x^{\xi 0}\bar{\psi}_\xi^2 + \bar{k}_y^{\xi 0}\bar{\psi}_\eta^2 \right]\Big|_{\xi=0} d\eta + \frac{1}{2}\int_0^1 \left[\bar{k}_w^{\xi 1}\bar{w}^2 + \bar{k}_x^{\xi 1}\bar{\psi}_\xi^2 + \bar{k}_y^{\xi 1}\bar{\psi}_\eta^2 \right]\Big|_{\xi=1} d\eta + \\ \frac{1}{2}\int_0^1 \left[\bar{k}_w^{\eta 0}\bar{w}^2 + \bar{k}_x^{\eta 0}\bar{\psi}_\xi^2 + \bar{k}_y^{\eta 0}\bar{\psi}_\eta^2 \right]\Big|_{\eta=0} d\xi + \frac{1}{2}\int_0^1 \left[\bar{k}_w^{\eta 1}\bar{w}^2 + \bar{k}_x^{\eta 1}\bar{\psi}_\xi^2 + \bar{k}_y^{\eta 1}\bar{\psi}_\eta^2 \right]\Big|_{\eta=1} d\xi, \end{array} \quad (11b)$$

$$T(\xi,\eta) = \frac{1}{2}\int_0^1\int_0^1 \left\{ \begin{array}{l} \left[\bar{w}^2 + \bar{I}_2\left(\bar{\psi}_\xi^2 + \bar{\psi}_\eta^2 \right) + \bar{l}_s^{\,2}\left(\frac{\partial\bar{w}}{\partial\xi} \right)^2 + \gamma^2\bar{l}_s^{\,2}\left(\frac{\partial\bar{w}}{\partial\eta} \right)^2 + \right. \\ \left. \bar{I}_2\bar{l}_s^{\,2}\left(\left(\frac{\partial\bar{\psi}_\xi}{\partial\xi} \right)^2 + \gamma^2\left(\frac{\partial\bar{\psi}_\xi}{\partial\eta} \right)^2 \right) + \bar{I}_2\bar{l}_s^{\,2}\left(\left(\frac{\partial\bar{\psi}_\eta}{\partial\xi} \right)^2 + \gamma^2\left(\frac{\partial\bar{\psi}_\eta}{\partial\eta} \right)^2 \right) \right] \end{array} \right\} d\xi d\eta, \quad (11c)$$

It can be noted that, by setting $\bar{l}_s = \bar{k}_w^{[*]} = \bar{k}_x^{[*]} = \bar{k}_y^{[*]} = 0$ in Eqs. (11a)-(11c), quadratic potential term

for the classical Mindlin plates can be retrieved.

2.2. Admissible displacement functions and Rayleigh-Ritz procedure

The selection of suitable admissible functions is crucial in the Rayleigh-Ritz method, as the accuracy of the solution depends heavily on how well these functions can represent the actual displacement. A major advantage of the quadratic functional given in Eq. (10) is that it significantly simplifies the determination of admissible displacement functions for the nanoplates. Any set of independent, complete basis functions can be utilized to achieve precise results. This is because the geometric BCs in the nanoplate are relaxed and enforced through translational and rotational boundary springs, which can be viewed as penalty parameters [62]. As a result, there is no explicit requirement to satisfy natural and essential conditions on these boundaries when determining the admissible displacement functions in advance. Herein, the Gram-Schmidt polynomials are introduced as admissible functions. Each of the displacement and rotation functions of the nanoplate, regardless of BCs, is stated as [51]:

$$\bar{w}(\xi,\eta)=\sum_{m=1}^{M}\sum_{n=1}^{N}\bar{W}_{mn}P_m(\xi)P_n(\eta), \tag{12a}$$

$$\bar{\psi}_{\xi}(\xi,\eta)=\sum_{m=1}^{M}\sum_{n=1}^{N}\bar{\Theta}_{mn}P_m(\xi)P_n(\eta), \tag{12b}$$

$$\bar{\psi}_{\eta}(\xi,\eta)=\sum_{m=1}^{M}\sum_{n=1}^{N}\bar{\Phi}_{mn}P_m(\xi)P_n(\eta), \tag{12c}$$

where M and N are the number of polynomial terms truncated in practical calculation $\bar{W}_{mn}$, $\bar{\Theta}_{mn}$ and $\bar{\Phi}_{mn}$ are corresponding Gram-Schmidt expansion coefficients, $P_m(\xi)$ and $P_n(\eta)$ denote the mth and nth order Gram-Schmidt polynomials for the displacement and rotation components in the interval [0, 1] across ξ and η directions, respectively, which are defined as [63]:

$$P_i(\tau)=\frac{\mathrm{P}_i(\tau)}{\sqrt{\int_0^1\left[\mathrm{P}_i(\tau)\right]^2 d\tau}},\quad \tau=\xi,\eta,\quad i=m,n, \tag{13}$$

where $\mathrm{P}_i(\tau)$ is an orthogonal polynomial set of functions. To address classical BCs, the first terms of the polynomials should be adjusted within the prescribed BCs. When it comes to general BCs, the first terms of the polynomials that meet the free BCs; i.e., $\mathrm{P}_1(\tau)=1$, are utilized. The following terms of the polynomial are derived using recursive equations described in [51], as follows:

$$\mathrm{P}_2(\tau)=(\tau-b_1)\mathrm{P}_1(\tau),\quad \mathrm{P}_{i+1}(\tau)=(\tau-b_i)\mathrm{P}_i(\tau)-c_i\mathrm{P}_{i-1}(\tau),\quad i\geq 2 \tag{14}$$

in which

$$b_i = \frac{\int_0^1 \tau \left[\mathrm{P}_i(\tau)\right]^2 d\tau}{\int_0^1 \left[\mathrm{P}_i(\tau)\right]^2 d\tau}, \qquad c_i = \frac{\int_0^1 \tau \mathrm{P}_{i-1}(\tau)\mathrm{P}_i(\tau) d\tau}{\int_0^1 \left[\mathrm{P}_{i-1}(\tau)\right]^2 d\tau}, \tag{15}$$

It is clear that the orthogonality condition is met by the constructed polynomials, i.e.,

$$\int_0^1 \mathrm{P}_i(\tau)\mathrm{P}_j(\tau) d\tau = \begin{cases} 0 & \text{if } i \neq j \\ 1 & \text{if } i = j \end{cases} \tag{16}$$

Substituting Eqs. (12a)-(12c) into Eqs. (11a)-(11d) and minimizing $\Pi(\xi,\eta)$ with respect to unknown expansion coefficients, i.e., $\partial\Pi(\xi,\eta)/\partial q = 0$ where $q = \bar{W}_{mn}$, $\bar{\Theta}_{mn}$ and $\bar{\Phi}_{mn}$, the following set of linear equations will be obtained:

$$[\mathbf{K} - \bar{\omega}^2 \mathbf{M}]\mathbf{q} = \mathbf{0}, \tag{17}$$

Here, $\mathbf{q}$ is a $1\times 3MN$ vector composed of the unknown coefficients as follows:

$$\mathbf{q} = \left\{\mathbf{q}^w, \mathbf{q}^\alpha, \mathbf{q}^\beta\right\}^T, \tag{18}$$

where

$$\mathbf{q}^w = \{\bar{W}_{11}, \bar{W}_{12}, \ldots, \bar{W}_{m1}, \bar{W}_{m2}, \ldots, \bar{W}_{mn}, \ldots, \bar{W}_{MN}\}, \tag{19a}$$

$$\mathbf{q}^\alpha = \{\bar{\Theta}_{11}, \bar{\Theta}_{12}, \ldots, \bar{\Theta}_{m1}, \bar{\Theta}_{m2}, \ldots, \bar{\Theta}_{mn}, \ldots, \bar{\Theta}_{MN}\}, \tag{19a}$$

$$\mathbf{q}^\beta = \{\bar{\Phi}_{11}, \bar{\Phi}_{12}, \ldots, \bar{\Phi}_{m1}, \bar{\Phi}_{m2}, \ldots, \bar{\Phi}_{mn}, \ldots, \bar{\Phi}_{MN}\}, \tag{19c}$$

$\mathbf{K}$ and $\mathbf{M}$ denote, in order, stiffness matrix and mass matrix with dimension of $3MN\times 3MN$ given by

$$\mathbf{K} = \begin{bmatrix} \mathbf{K}^{ww} & \mathbf{K}^{w\alpha} & \mathbf{K}^{w\beta} \\ \mathbf{K}^{\alpha w} & \mathbf{K}^{\alpha\alpha} & \mathbf{K}^{\alpha\beta} \\ \mathbf{K}^{\beta w} & \mathbf{K}^{\beta\alpha} & \mathbf{K}^{\beta\beta} \end{bmatrix}, \quad \mathbf{M} = \begin{bmatrix} \mathbf{M}^{ww} & \mathbf{0} & \mathbf{0} \\ \mathbf{0} & \mathbf{M}^{\alpha\alpha} & \mathbf{0} \\ \mathbf{0} & \mathbf{0} & \mathbf{M}^{\beta\beta} \end{bmatrix}, \tag{20}$$

where the elements of the above matrices have been provided in the Appendix. Eq. (17) represents a standard eigenproblem that can be solved to determine the natural frequencies of the nanoplate. Also, the eigenvector $\mathbf{q}$ presents the vibration mode shape. We have summarized the solution procedure in the flowchart shown in Fig. 2.

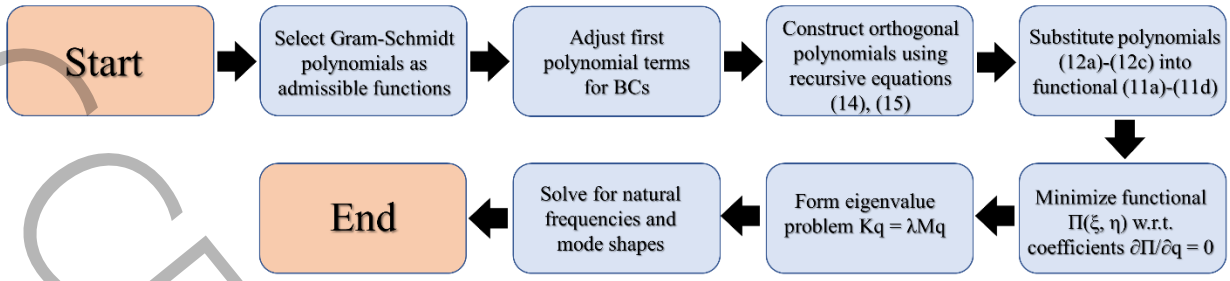

Fig. 2. Flowchart of the proposed method.

3. Results and discussion

This section addresses the proposed model's capabilities in predicting the vibrational frequencies of nanoplates with arbitrary BCs. First, the convergence of the Rayleigh-Ritz solutions is investigated in terms of the number of polynomial terms used. Next, the efficiency and accuracy of the proposed method for the free vibration of nanoplates with classical BCs are verified against existing literature. Finally, a parametric study is performed for nanoplates subjected to elastic BCs.

For the sake of brevity, symbolic notations are utilized to define the BCs of the four edges. For instance, "CSFS" indicates that BCs at $\eta = 0$, $\xi = 1$, $\eta = 1$, and $\xi = 0$ are clamped, simply-supported, free, and simply-supported, respectively. In the calculations, the following material properties are adopted: Young's modulus $E = 1.06\,\text{TPa}$, density $\rho = 2300\text{kg}/\text{m}^3$, Poisson's ratio $\nu = 0.3$ and shear correction factor $k_s = 0.86667$. Additionally, the vibrational behavior of the nanoplate is described through the dimensionless frequency parameter $\overline{\Omega} = \omega a^2\sqrt{\rho h / D}$, where ω is the natural frequency.

As stated in Section 2, the arbitrary BCs of the nanoplate are enforced through the incorporation of a set of continuously distributed translational springs and two sets of rotational springs along each edge of the nanoplate. This allows for the simulation of arbitrary BCs by assigning appropriate stiffnesses to the boundary springs. In the present study, the vibration frequencies of nanoplates under various BCs are determined, including classical BCs such as simply supported (S), clamped (C), and free (F), as well as elastic BCs denoted as E^1, E^2 and E^3, and their combinations. The dimensionless spring stiffness parameters for the three classical BCs and the three elastic BCs are provided below:

F edge: $\bar{k}_w^{[*]} = \bar{k}_x^{[*]} = \bar{k}_y^{[*]} = 0, \quad [*] = \xi_0, \xi_1, \eta_0, \eta_1,$

S edge: $\bar{k}_w^{[*]} = \bar{k}_y^{[*]} = 10^5, \quad \bar{k}_x^{[*]} = 0, \quad [*] = \xi_0, \xi_1, \quad \bar{k}_w^{[*]} = \bar{k}_x^{[*]} = 10^5, \quad \bar{k}_y^{[*]} = 0, \quad [*] = \eta_0, \eta_1,$

C edge: $\bar{k}_w^{[*]} = \bar{k}_x^{[*]} = \bar{k}_y^{[*]} = 10^5, \quad [*] = \xi_0, \xi_1, \eta_0, \eta_1,$

E^1 edge: $\bar{k}_w^{[*]} = \bar{k}_x^{[*]} = \bar{k}_y^{[*]} = 0.03, \quad [*] = \xi_0, \xi_1, \eta_0, \eta_1,$

E^2 edge: $\bar{k}_x^{[*]} = \bar{k}_y^{[*]} = 10^5, \quad \bar{k}_w^{[*]} = 0.03, \quad [*] = \xi_0, \xi_1, \ \bar{k}_x^{[*]} = \bar{k}_y^{[*]} = 10^5, \quad \bar{k}_w^{[*]} = 0.03, \quad [*] = \eta_0, \eta_1,$

E^3 edge: $\bar{k}_x^{[*]} = \bar{k}_y^{[*]} = 0.03, \quad \bar{k}_w^{[*]} = 10^5, \quad [*] = \xi_0, \xi_1, \ \bar{k}_x^{[*]} = \bar{k}_y^{[*]} = 0.03, \quad \bar{k}_w^{[*]} = 10^5, \quad [*] = \eta_0, \eta_1,$

It is important to note that the value of the nonlocal factor depends on several parameters, including material type, internal characteristic length, boundary conditions, nanoplate dimensions, and mode number. When considering graphene sheets as nanoplates, studies have shown that the material constant e_0 for zigzag graphene sheets ranges from 3 to 8, as identified through theoretical analysis and molecular dynamics simulations in Ref. [64]. Given the C-C bond length of approximately 0.142 nm or the lattice parameter of graphene at 0.246 nm, the nonlocal factor value falls within the range of 0 to 2 nm. This range is consistent with findings from other studies using molecular dynamics simulations and size-dependent plate models. Based on this explanation, we adopt a nonlocal factor range of 0 to 2 nm for this study [65-67].

3.1. Convergence analysis

Given that a finite truncation number of polynomial terms must be used in the displacement expressions for practical calculations, the presented method should be regarded as a method with arbitrary accuracy. Therefore, it is crucial to thoroughly assess the convergence and numerical robustness of the method's solution. In Table 1, the dimensionless fundamental frequencies of the nonlocal Mindlin nanoplate subjected to various classical BCs are listed. In Table 2, the dimensionless natural frequencies of nanoplates for higher modes with various classical BCs are presented. The results demonstrate that, with an increase in truncation terms, the solutions converge rapidly for all nanoplates with different BCs for fundamental frequencies. However, for higher modes, more truncation terms are required to achieve convergence. The efficiency of the Gram-Schmidt polynomial series solution in achieving convergence of the natural frequencies is evident in the tabulated results in Tables 1 and 2. Considering the high computational cost of using large truncation terms, we adopt $M, N = 10$ to achieve adequate convergence in analyzing the problem at hand.

Table 1 Convergence of dimensionless fundamental frequency $\bar{\Omega}_1$ for nanoplates with various classical BCs ($N = M, a = b = 20$ nm, $l_s = 2$ nm, h=0.34 nm).

BCs	$N=5$	$N=6$	$N=7$	$N=8$	$N=9$	$N=10$	$N=11$	$N=12$	$N=13$	$N=14$
CCCC	32.229	32.228	32.201	32.200	32.197	32.197	32.196	32.196	32.196	32.196
SSSS	18.023	18.023	18.020	18.021	18.021	18.021	18.021	18.021	18.021	18.021

CSCS	28.606	28.603	28.588	28.588	28.585	28.585	28.585	28.585	28.585	28.585
CCFF	6.678	6.671	6.663	6.659	6.656	6.654	6.652	6.650	6.649	6.649
FSFS	14.424	14.387	14.360	14.357	14.353	14.352	14.351	14.350	14.349	14.349
SSFF	3.276	3.275	3.274	3.273	3.272	3.272	3.271	3.270	3.269	3.269

Table 2 Convergence of dimensionless natural frequencies for higher modes $\overline{\Omega}_3$ and $\overline{\Omega}_5$ of nanoplates with various classical BCs ($N=M$, $a=b=20$ nm, $l_s=2$ nm, h=0.34 nm).

BCs	$\overline{\Omega}_3$						$\overline{\Omega}_5$					
	$N=6$	$N=7$	$N=8$	$N=9$	$N=10$	$N=11$	$N=6$	$N=7$	$N=8$	$N=9$	$N=10$	$N=11$
CCCC	59.14	59.09	58.17	58.16	58.15	58.15	462.18	94.78	90.57	89.88	89.87	89.86
SSSS	40.39	40.38	40.28	40.28	40.28	40.28	94.22	70.55	70.51	69.67	69.67	69.67
CCSS	49.44	49.17	48.89	48.88	48.88	48.88	120.03	82.78	81.23	79.59	79.50	79.49
CSSF	43.15	42.73	42.37	42.35	42.34	42.34	52.33	52.14	51.93	51.91	51.90	51.89
SFSF	29.27	29.08	29.07	29.06	29.05	29.05	37.98	37.98	37.95	37.85	37.84	37.84
SSFF	17.04	17.01	17.01	17.01	17.01	17.01	38.74	38.61	38.38	38.37	38.36	38.36

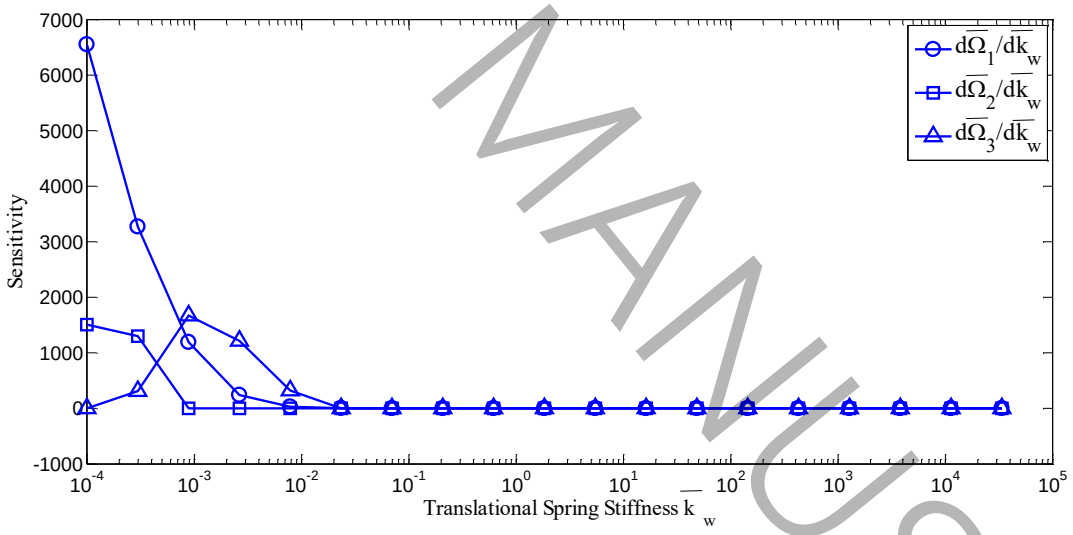

Fig. 3. Sensitivity of the first three dimensionless frequencies to $\bar{k}_w^{0\xi}$ for SFSF ($a=b=20$ nm, $h=0.34$ nm, $l_s=2$ nm).

To further evaluate the numerical robustness of the Gram-Schmidt polynomial series solution, a sensitivity analysis is conducted to assess the impact of the translational spring stiffness $\bar{k}_w^{0\xi}$ on the first three dimensionless natural frequencies $(\overline{\Omega}_1, \overline{\Omega}_2, \overline{\Omega}_3)$ for SFSF with $M, N=10$. The sensitivity, defined as $\mathrm{d}\overline{\Omega}_i / \mathrm{d}\bar{k}_w^{0\xi}$, and the relative change, $\dfrac{\Delta\overline{\Omega}_i / \overline{\Omega}_i}{\Delta\bar{k}_w^{0\xi} / \bar{k}_w^{0\xi}}$, are computed

over a range of $\bar{k}_w^{0\xi}$ from 10^{-4} to 10^{5} using central finite differences. Fig. 3 illustrates the sensitivity, showing a high initial value at low $\bar{k}_w^{0\xi}$ (i.e., 10−4) that decreases sharply and levels off toward zero at higher stiffness, with no distinct peaks in the range shown. Fig. 4 presents the relative change which highlights regions where small stiffness variations cause substantial frequency shifts. These results confirm the method's stability, as sensitivities diminish at extreme stiffness values, and validate the choice of $M, N = 10$ for reliable frequency predictions in the SFSF BCs.

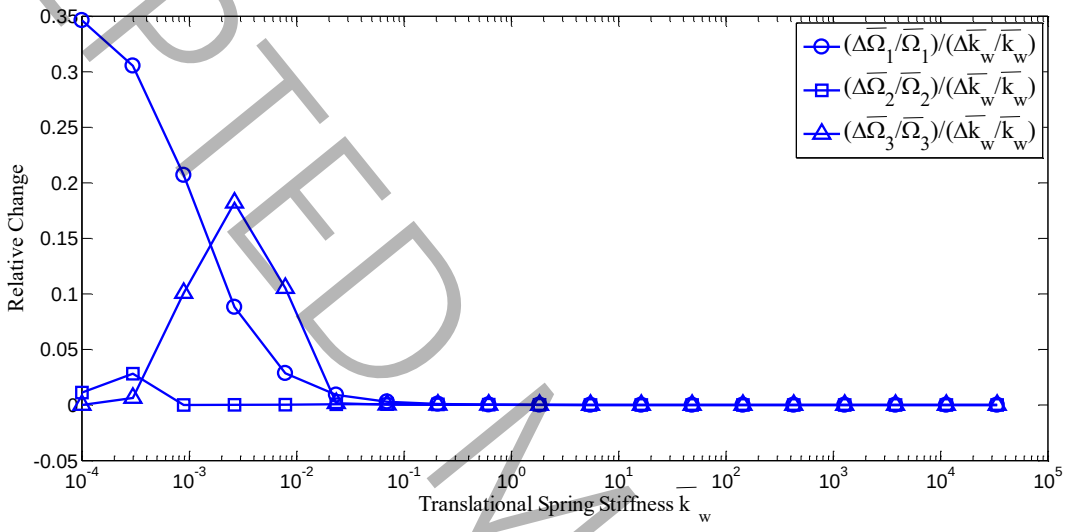

Fig. 4. Relative change in the first three dimensionless frequencies to $\bar{k}_w^{0\xi}$ for SFSF ($a = b = 20$ nm, $h = 0.34$ nm, $l_s = 2$ nm).

Table 3 Comparison of dimensionless fundamental frequency $\bar{\Omega}_1$ for nanoplates with various classical BCs ($a = b = 5$ nm).

BCs	Model	$l_s = 0$ nm	$l_s = 1$ nm	$l_s = \sqrt{2}$ nm	$l_s = 2$ nm
SSSS	Present	19.7113	14.7348	12.2739	9.6664
	Chakraverty et al. [35]	19.7000	14.7556	12.2912	9.6800
	Wang et al. [50]	19.7392	14.7556	12.2912	9.6800
CCCC	Present	35.8231	25.5102	20.8431	16.1401
	Chakraverty et al. [35]	36	25.6182	20.9293	16.2072
	Wang et al. [50]	35.9990	25.6337	20.9443	16.2207
SCSC	Present	28.8486	21.0384	17.3515	13.5469
	Chakraverty et al. [35]	29	21.1091	17.4090	13.5914
	Wang et al. [50]	28.9509	21.1091	17.4090	13.5914

FCFC	Present	22.0982	17.9848	15.1963	11.7139
	Chakraverty et al. [35]	22.2000	18.0585	15.2936	11.7908
	Wang et al. [50]	22.2244	18.0916	15.3174	11.8124

3.2. Verification study

Having established the mathematical model and nonlocal methodology in the preceding section, we now proceed to validate the efficiency, reliability and accuracy of the proposed formulation for the free vibration analysis of nanoplates. This is achieved by comparing the calculated results obtained using our approach with those reported in the existing literature. In the first comparison shown in Table 3, the dimensionless fundamental frequencies for nonlocal Mindlin nanoplates with various classical BCs and different nonlocal factors are detailed. The comparison reveals that the present solutions match very well with the results obtained using the Rayleigh-Ritz method and iterative separation-of-variable method based on the NKP model, as reported by Chakraverty et al. [35] and Wang et al. [50], respectively. The negligible discrepancies, which do not exceed 0.84% even in the worst case, can be attributed to the use of different plate theories and the shear effects in NMP that are not incorporated in NKP.

In the second comparison, Table 4 lists the first four dimensionless frequencies $\overline{\Omega}$ for the nanostructure with various classical BCs. The comparisons are performed between the present results and the extended separation-of-variable method reported by Li et al. [59], who used the NMP model. The table demonstrates reasonable agreement between the present results and the referential data.

It should be noted that to validate the theoretical results presented here, experimental methods such as Atomic Force Microscopy (AFM) and laser vibrometry, along with other approaches, can be employed as well to measure the vibrational characteristics of nanoplates. These methods enable a direct comparison with the proposed nonlocal Mindlin plate model.

Table 4 Comparison of first four dimensionless frequency $\overline{\Omega}$ for nanoplates with various classical BCs ($a=b=10$ nm, h=1 nm).

BCs	l_s(nm)	Model	Mode			
			1	2	3	4
CCCC	1	Present	29.3639	50.0221	50.0221	64.0816
		Li et al. [59]	29.3875	50.0369	50.0369	64.0999
	2	Present	23.3667	34.6404	34.6404	41.2909
		Li et al. [59]	23.3911	34.6552	34.6552	41.3107
CCSS	1	Present	22.9311	43.3584	43.6915	58.0828
		Li et al. [59]	22.9390	43.5326	43.5326	58.0968
	2	Present	18.4353	30.3263	30.6447	37.7483
		Li et al. [59]	18.4433	30.4946	30.4946	37.7652
CFFF	1	Present	3.3546	7.5370	17.3548	21.0591
		Li et al. [59]	3.3938	7.5820	18.0779	20.7710

	2	Present	3.1482	6.3923	12.9402	15.2315
		Li et al. [59]	3.1872	6.4317	13.8362	14.6142
CSSF	1	Present	14.9680	24.6598	38.2263	42.6727
		Li et al. [59]	15.0125	24.6806	38.2862	42.6979
	2	Present	12.7175	18.2618	27.2371	28.1448
		Li et al. [59]	12.7577	18.2837	27.3027	28.1623
SSSF	1	Present	10.7127	22.4735	32.0821	41.5970
		Li et al. [59]	10.7110	22.4660	32.0754	41.5791
	2	Present	9.2365	16.7286	23.1916	27.5472
		Li et al. [59]	9.2348	16.7219	23.1836	27.5403
SSFF	1	Present	3.2007	14.4873	16.3845	28.7161
		Li et al[٥٩] .	3.2156	15.6062	15.6062	28.9499
	2	Present	2.9734	11.0253	12.7347	20.1256
		Li et al[٥٩] .	2.9877	12.0187	12.0187	20.3908
SFSF	1	Present	9.0048	13.9675	27.0518	30.7660
		Li et al. [59]	9.0045	13.9580	27.0435	30.7632
	2	Present	7.9771	11.2459	18.6238	22.5160
		Li et al. [59]	7.9768	11.2374	18.6172	22.5127

3.3. Parametric study

The developed methodology, following comprehensive convergence and validation analyses, is employed to determine the impacts of boundary spring stiffness and the nonlocal factor on the free vibration of the nanoplates. Fig. 5 shows the 1^{st}, 2^{nd} and 3^{rd} dimensionless frequencies against boundary spring stiffness. The nanoplate under consideration has completely free boundaries at $\eta = 0$ and $\eta = 1$, while the $\xi = 0$ boundary is clamped. At the $\xi = 1$ edge, the nanoplate is elastically supported by a single set of spring components, with stiffnesses ranging from 10^{-8} to 10^{5}. Examining Fig. 5 reveals that the dimensionless frequencies remain relatively constant as long as the stiffness parameters of the boundary springs are less than 10^{-3}. This low stiffness regime indicates that the boundary at $\xi = 1$ behaves like a free edge, as long as the stability of the proposed methods is maintained. In this case, the springs provide negligible resistance which allows vibrations to be governed by the nanoplate's properties. However, a distinct change occurs as the stiffness parameters are increased beyond that threshold. In this regime, the dimensionless frequencies begin to rise sharply. Notably, once the stiffness parameters surpass 10^{3}, the dimensionless frequencies approach a maximum value and remain unchanged. In this high stiffness regime, the boundary at $\xi = 1$ acts as a clamped edge, with the springs fully constraining displacements and rotations, stabilizing the vibrational modes.

To further demonstrate the effects of stiffness parameters on the dimensionless natural frequencies, we have plotted the dimensionless fundamental frequency against the boundary spring stiffness in Fig. 6. This

figure shows the development of the first three dimensionless frequencies as the stiffnesses of the translational and rotational artificial springs at the boundaries vary from zero (free edge at $\xi = 1$) to infinity (clamped edge at $\xi = 1$). It is important to note that the same BCs mentioned earlier are applied in this figure as well. The key observation from Fig. 6 is that when the spring stiffness value exceeds 10^2, the natural frequencies of the nanoplate converge to a fixed value. This convergence reflects a clamped-like behavior at $\xi = 1$, where high spring stiffness restricts all boundary motion, with rotational springs having a more pronounced effect on higher frequencies.

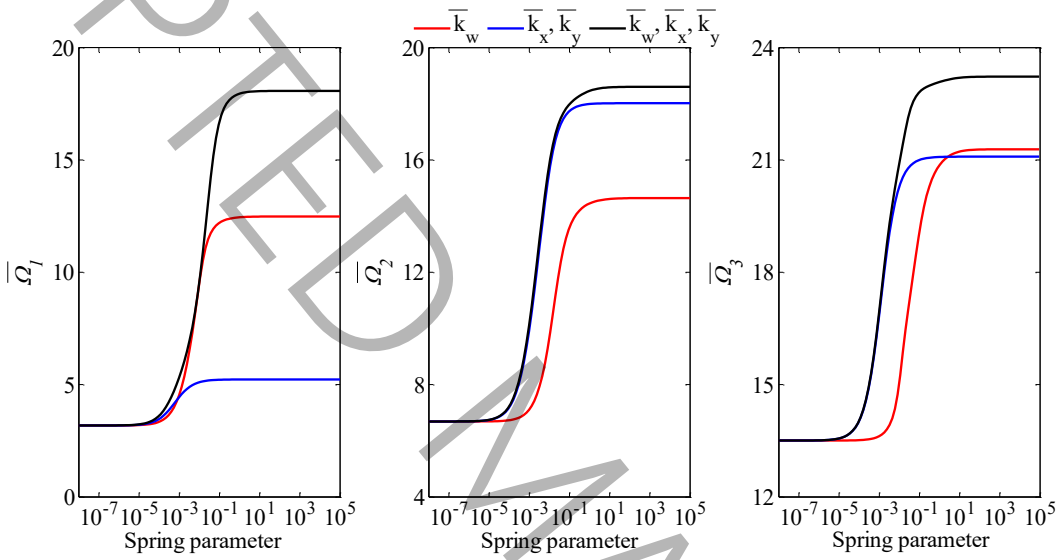

Fig. 5. The first three dimensionless frequencies versus boundary springs stiffness ($a = b = 10$ nm, $h = 0.34$ nm, $l_s = 2$ nm).

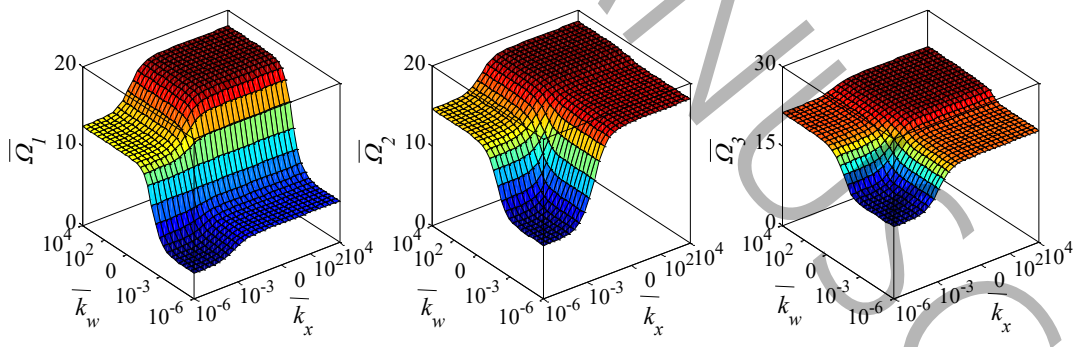

Fig. 6. Surface plot of the first three dimensionless frequencies versus boundary springs stiffness ($a = b = 10$ nm, h=0.34 nm, l_s=2 nm, $\bar{k}_x^{\xi} = \bar{k}_y^{\xi}$).

In another study, the dimensionless fundamental frequencies of the nanoplates with various classical-elastic combined BCs are presented in Table 5. The table examines nine sets of BCs, including the TIFTIF,

ΠSΠS, and ΠCΠC conditions, where Π denotes E^1, E^2, and E^3. Analysis of the data in Table 5 reveals that E^1FE^1F BCs are associated with the lowest fundamental frequencies, while E^3CE^3C conditions correspond to the highest frequencies. Furthermore, the influence of the nonlocal factor is observed to be minimal for E^1FE^1F case, but it has the most substantial impact on E^3CE^3C conditions.

Table 5 The dimensionless fundamental frequency $\bar{\Omega}_1$ for nanoplates with various classical-elastic combined BCs ($a = b = 10$ nm, $h = 0.34$ nm).

l_s(nm)	E^1FE^1F	E^2FE^2F	E^3FE^3F	E^1SE^1S	E^2SE^2S	E^3SE^3S	E^1CE^1C	E^2CE^2C	E^3CE^3C
0	11.9178	12.0588	21.1194	22.3634	23.9363	27.8578	30.5639	31.7915	34.8616
0.5	11.9028	12.0450	20.8085	21.9935	23.5082	27.1398	29.9736	31.1362	33.8795
1	11.8569	12.0027	19.9480	20.9747	22.3360	25.2759	28.3606	29.3543	31.3559
1.5	11.7765	11.9285	18.7132	19.5286	20.6915	22.8688	26.1034	26.8911	28.1510
2	11.6556	11.8165	17.2974	17.9017	18.8681	20.4176	23.6198	24.2219	24.9485

Given the importance of the nonlocal factor and its effects on the vibrational analysis of nanoplates, we have plotted the dimensionless fundamental frequencies against the nonlocal factor in Fig. 7 for various classical-elastic BCs. The predicted results show that, for all the considered BCs, the fundamental frequencies decrease as the nonlocal factor increases. However, the degree of this frequency reduction varies depending on the specific BCs. Nanoplates with CCCC and $E^3E^3E^3E^3$ BCs exhibit a more pronounced sensitivity to the increase in the nonlocal factor, compared to the $E^1E^1E^1E^1$ and $E^2E^2E^2E^2$ cases. Additionally, it is observed that when the nonlocal factor is zero, the fundamental frequencies for the SSSS BCs are greater than those for $E^1E^1E^1E^1$ and $E^2E^2E^2E^2$ cases. However, as the nonlocal factor increases, the discrepancies among these BCs diminish. In fact, when the nonlocal factor exceeds 1.1 nm, the fundamental frequencies for SSSS BCs become higher than those for $E^1E^1E^1E^1$ and $E^2E^2E^2E^2$ cases.

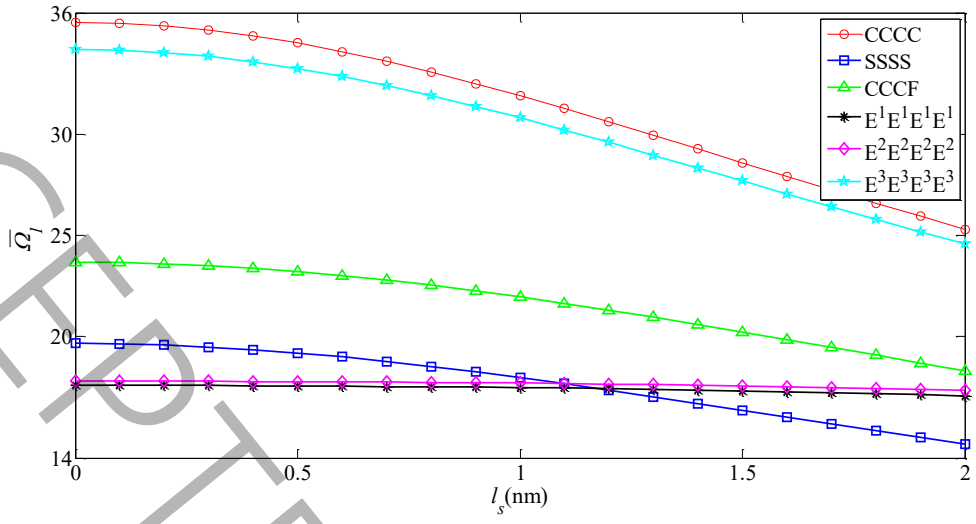

Fig. 7. The dimensionless fundamental frequency versus nonlocal factor for various classical and elastic BCs ($a = b = 10$ nm, $h = 0.34$ nm).

4. Conclusions

This paper presents a unified approach for the free vibration analysis of nonlocal Mindlin nanoplates using the weighted residual method based on the artificial spring technique. The study employed the Gram-Schmidt polynomial series as admissible displacement functions and applied the Rayleigh-Ritz method to solve the eigenvalue problems for the vibration of nanoplates with arbitrary BCs. The proposed method was validated by comparing the numerical results with existing literature. The study investigated the vibrational frequencies of nanoplates under various classical BCs, elastic BCs, and their combinations, and examined the effects of the spring stiffness parameters on the vibration characteristics. The main findings of this work are summarized as follows:

1. The proposed method effectively computes the natural frequencies of nanoplates with arbitrary BCs, including classical BCs, elastic BCs, and their combinations, while capturing size-dependent behavior at the nanoscale.
2. The fundamental frequency of the nanoplates converges rapidly with an increasing number of truncation terms for various BCs; however, for higher modes, more truncation terms are required to achieve accuracy.
3. For a specific BC, a sensitivity analysis indicates that the natural frequencies are highly sensitive to translational spring stiffness at very low values, which stabilizes as the stiffness increases, confirming the stability and reliability of the proposed method.
4. The impact of the rotational spring parameters is more pronounced on the second and third dimensionless natural frequencies compared to the first dimensionless natural frequency.

5. The nonlocal factor has a minimal impact on the dimensionless fundamental frequency of nanoplates with $E^1E^1E^1E^1$ and $E^2E^2E^2E^2$ elastic BCs, whereas its influence is more pronounced for those with CCCC, SSSS, and $E^3E^3E^3E^3$ BCs.

The novel technique introduced in this study enables bending, vibration, and buckling analyses of nanostructures, such as nanoplates, nanoshells and circular nanoplates, using advanced nonlocal continuum models. Furthermore, the current model is limited to linear vibration analysis, suitable for small-amplitude oscillations. Nanoplates may exhibit nonlinear geometric and material behavior in practical applications. Investigating nonlinear vibrational characteristics with elastic BCs, including geometric nonlinearity, nonlinear boundary stiffness, and amplitude-dependent frequencies, presents an exciting avenue for future research.

Appendix

This appendix provides the entries of the matrices **K** and **M** for the nanoplate with arbitrary BCs. In order to simplify and clarify the expressions, two indexes are pre-defined:

$$s = N(i-1)+k, \quad q = N(j-1)+l, \tag{A.1}$$

where $i, j \in [1, M]$ and $k, l \in [1, N]$.

The entries of the stiffness matrix **K** are computed using the following formulations:

$$\mathbf{K}_{sq}^{ww} = \int_0^1 \left(\frac{dP_i(\xi)}{d\xi} \frac{dP_j(\xi)}{d\xi} \right) d\xi \int_0^1 P_k(\eta) P_l(\eta) d\eta + \gamma^2 \int_0^1 P_i(\xi) P_j(\xi) d\xi \int_0^1 \left(\frac{dP_k(\eta)}{d\eta} \frac{dP_l(\eta)}{d\eta} \right) d\eta +$$

$$+ \int_0^1 P_k(\eta) P_l(\eta) d\eta \left(\bar{k}_w^{\xi_0} P_i(\xi) P_j(\xi) \Big|_{\xi=0} + \bar{k}_w^{\xi_1} P_i(\xi) P_j(\xi) \Big|_{\xi=1} \right) + \int_0^1 P_i(\xi) P_j(\xi) d\xi \begin{pmatrix} \bar{k}_w^{\eta_0} P_k(\eta) P_l(\eta) \Big|_{\eta=0} \\ + \bar{k}_w^{\eta_1} P_k(\eta) P_l(\eta) \Big|_{\eta=1} \end{pmatrix}, \tag{A.2}$$

$$\mathbf{K}_{sq}^{w\alpha} = -\int_0^1 \left(\frac{dP_i(\xi)}{d\xi} P_j(\xi) \right) d\xi \int_0^1 P_k(\eta) P_l(\eta) d\eta, \tag{A.3}$$

$$\mathbf{K}_{sq}^{w\beta} = -\gamma \int_0^1 P_i(\xi) P_j(\xi) d\xi \int_0^1 \left(\frac{dP_k(\eta)}{d\eta} P_l(\eta) \right) d\eta, \tag{A.4}$$

$$\mathbf{K}_{sq}^{\alpha\alpha}=\int_0^1 P_i(\xi)P_j(\xi)d\xi\int_0^1 P_k(\eta)P_l(\eta)d\eta+\frac{(1-\nu)\gamma^2\bar{D}}{2}\int_0^1 P_i(\xi)P_j(\xi)d\xi\int_0^1\left(\frac{dP_k(\eta)}{d\eta}\frac{dP_l(\eta)}{d\eta}\right)d\eta+$$
$$+\bar{D}\int_0^1\left(\frac{dP_i(\xi)}{d\xi}\frac{dP_j(\xi)}{d\xi}\right)d\xi\int_0^1 P_k(\eta)P_l(\eta)d\eta+\int_0^1 P_k(\eta)P_l(\eta)d\eta\left(\begin{matrix}\bar{k}_x^{\xi_0}P_i(\xi)P_j(\xi)\big|_{\xi=0}+\\ \bar{k}_x^{\xi_1}P_i(\xi)P_j(\xi)\big|_{\xi=1}\end{matrix}\right)+ \tag{A.5}$$
$$\int_0^1 P_i(\xi)P_j(\xi)d\xi\left(\bar{k}_x^{\eta_0}P_k(\eta)P_l(\eta)\big|_{\eta=0}+\bar{k}_x^{\eta_1}P_k(\eta)P_l(\eta)\big|_{\eta=1}\right),$$

$$\mathbf{K}_{sq}^{\beta\beta}=\int_0^1 P_i(\xi)P_j(\xi)d\xi\int_0^1 P_k(\eta)P_l(\eta)d\eta+\gamma^2\bar{D}\int_0^1 P_i(\xi)P_j(\xi)d\xi\int_0^1\left(\frac{dP_k(\eta)}{d\eta}\frac{dP_l(\eta)}{d\eta}\right)d\eta+$$
$$\frac{(1-\nu)\bar{D}}{2}\int_0^1\left(\frac{dP_i(\xi)}{d\xi}\frac{dP_j(\xi)}{d\xi}\right)d\xi\int_0^1 P_k(\eta)P_l(\eta)d\eta+\int_0^1 P_k(\eta)P_l(\eta)d\eta\left(\begin{matrix}\bar{k}_y^{\xi_0}P_i(\xi)P_j(\xi)\big|_{\xi=0}+\\ \bar{k}_y^{\xi_1}P_i(\xi)P_j(\xi)\big|_{\xi=1}\end{matrix}\right)+ \tag{A.6}$$
$$\int_0^1 P_i(\xi)P_j(\xi)d\xi\left(\bar{k}_y^{\eta_0}P_k(\eta)P_l(\eta)\big|_{\eta=0}+\bar{k}_y^{\eta_1}P_k(\eta)P_l(\eta)\big|_{\eta=1}\right),$$

$$\mathbf{K}_{sq}^{\alpha\beta}=\bar{D}\nu\gamma\int_0^1\left(\frac{dP_i(\xi)}{d\xi}P_j(\xi)\right)d\xi\int_0^1 P_k(\eta)\left(\frac{dP_l(\eta)}{d\eta}\right)d\eta+$$
$$\frac{(1-\nu)\gamma\bar{D}}{2}\int_0^1 P_i(\xi)\left(\frac{dP_j(\xi)}{d\xi}\right)d\xi\int_0^1\left(\frac{dP_k(\eta)}{d\eta}P_l(\eta)\right)d\eta \tag{A.7}$$

$$\mathbf{K}_{sq}^{\alpha w}=-\int_0^1\left(\frac{dP_j(\xi)}{d\xi}P_i(\xi)\right)d\xi\int_0^1 P_l(\eta)P_k(\eta)d\eta, \tag{A.8}$$

$$\mathbf{K}_{sq}^{\beta w}=-\gamma\int_0^1 P_j(\xi)P_i(\xi)d\xi\int_0^1\left(\frac{dP_l(\eta)}{d\eta}P_k(\eta)\right)d\eta, \tag{A.9}$$

$$\mathbf{K}_{sq}^{\beta\alpha}=\bar{D}\nu\gamma\int_0^1\left(\frac{dP_j(\xi)}{d\xi}P_i(\xi)\right)d\xi\int_0^1 P_l(\eta)\left(\frac{dP_k(\eta)}{d\eta}\right)d\eta+$$
$$\frac{(1-\nu)\gamma\bar{D}}{2}\int_0^1 P_j(\xi)\left(\frac{dP_i(\xi)}{d\xi}\right)d\xi\int_0^1\left(\frac{dP_l(\eta)}{d\eta}P_k(\eta)\right)d\eta, \tag{A.10}$$

and the entries of the mass matrix **M** are computed based on the following formulations:

$$\mathbf{M}^{ww}=\int_0^1 P_i(\xi)P_j(\xi)d\xi\int_0^1 P_k(\eta)P_l(\eta)d\eta+\bar{l}_s^{\,2}\begin{pmatrix}\int_0^1\left(\frac{dP_i(\xi)}{d\xi}\frac{dP_j(\xi)}{d\xi}\right)d\xi\int_0^1 P_k(\eta)P_l(\eta)d\eta+\\ \gamma^2\int_0^1 P_i(\xi)P_j(\xi)d\xi\int_0^1\left(\frac{dP_k(\eta)}{d\eta}\frac{dP_l(\eta)}{d\eta}\right)d\eta\end{pmatrix}, \tag{A.11}$$

$$\mathbf{M}^{\alpha\alpha}=\mathbf{M}^{\beta\beta}=\bar{I}_2\int_0^1 P_i(\xi)P_j(\xi)d\xi\int_0^1 P_k(\eta)P_l(\eta)d\eta+\bar{l}_s^{\,2}\bar{I}_2\begin{pmatrix}\int_0^1\left(\frac{dP_i(\xi)}{d\xi}\frac{dP_j(\xi)}{d\xi}\right)d\xi\int_0^1 P_k(\eta)P_l(\eta)d\eta+\\ \gamma^2\int_0^1 P_i(\xi)P_j(\xi)d\xi\int_0^1\left(\frac{dP_k(\eta)}{d\eta}\frac{dP_l(\eta)}{d\eta}\right)d\eta\end{pmatrix} \tag{A.12}$$

References

[1] K.E. Whitener Jr, P.E. Sheehan, Graphene synthesis, Diamond and related materials, 46 (2014) 25-34.

[2] B.K. Choi, J. Kim, Z. Luo, J. Kim, J.H. Kim, T. Hyeon, S. Mehraeen, S. Park, J. Park, Shape transformation mechanism of gold nanoplates, ACS nano, 17(3) (2023) 2007-2018.

[3] J. Chen, S. Li, Y. Chen, J. Yang, J. Dong, X. Lu, l-cysteine-terminated triangular silver nanoplates/MXene nanosheets are used as electrochemical biosensors for efficiently detecting 5-hydroxytryptamine, Analytical Chemistry, 93(49) (2021) 16655-16663.

[4] Y. Zhao, M. Zhao, X. Ding, Z. Liu, H. Tian, H. Shen, X. Zu, S. Li, L. Qiao, One-step colloid fabrication of nickel phosphides nanoplate/nickel foam hybrid electrode for high-performance asymmetric supercapacitors, Chemical Engineering Journal, 373 (2019) 1132-1143.

[5] R. Ding, S. Chen, J. Lv, W. Zhang, X.-d. Zhao, J. Liu, X. Wang, T.-j. Gui, B.-j. Li, Y.-z. Tang, Study on graphene modified organic anti-corrosion coatings: A comprehensive review, Journal of Alloys and Compounds, 806 (2019) 611-635.

[6] W. Chen, S. Luo, M. Sun, X. Wu, Y. Zhou, Y. Liao, M. Tang, X. Fan, B. Huang, Z. Quan, High-entropy intermetallic PtRhBiSnSb nanoplates for highly efficient alcohol oxidation electrocatalysis, Advanced Materials, 34(43) (2022) 2206276.

[7] H. Hu, H. Li, Y. Lei, J. Liu, X. Liu, R. Wang, J. Peng, X. Wang, Mg-doped LiMn0. 8Fe0. 2PO4/C nano-plate as a high-performance cathode material for lithium-ion batteries, Journal of Energy Storage, 73 (2023) 109006.

[8] M. Guerroudj, A. Drai, A.A. Daikh, M.S.A. Houari, B. Aour, M.A. Eltaher, M.-O. Belarbi, Size-dependent free vibration analysis of multidirectional functionally graded nanobeams via a nonlocal strain gradient theory, Journal of Engineering Mathematics, 146 (2024) 20.

[9] I. Jafarsadeghi-Pournaki, G. Rezazadeh, R. Shabani, Nonlinear instability modeling of a nonlocal strain gradient functionally graded capacitive nanobridge in thermal environment, International Journal of Applied Mechanics, 10 (2018) 1850083.

[10] Z. Rahimi, G. Rezazadeh, W. Sumelka, A nonlocal fractional stress–strain gradient theory, International Journal of Mechanics and Materials in Design, 16 (2020) 265–278.

[11] B. Mawphlang, P. Patra, Study of the large bending behavior of CNTs using LDTM and nonlocal elasticity theory, International Journal of Non-Linear Mechanics, 166 (2024) 104828.

[12] S. Valilou, G. Rezazadeh, R. Shabani, M. Fathalilou, Bifurcation analysis of a capacitive microresonator considering nonlocal elasticity theory, International Journal of Nonlinear Sciences and Numerical Simulation, 15 (2014) 241–249.

[13] G. Rezazadeh, M. Sheikhlou, R. Shabani, Analysis of bias DC voltage effect on thermoelastic damping ratio in short nanobeam resonators based on nonlocal elasticity theory and dual-phase-lagging heat conduction model, Meccanica, 50 (2015) 2963–2976.

[14] M. Al-Furjan, M. Xu, A. Farrokhian, G.S. Jafari, X. Shen, R. Kolahchi, On wave propagation in piezoelectric-auxetic honeycomb-2D-FGM micro-sandwich beams based on modified couple stress and refined zigzag theories, Waves in Random and Complex Media, 35(1) (2025) 1147-1171.

[15] S. Dastjerdi, F. Naeijian, B. Akgöz, Ö. Civalek, On the mechanical analysis of microcrystalline cellulose sheets, International Journal of Engineering Science, 166 (2021) 103500.
[16] Ş.D. Akbaş, S. Dastjerdi, B. Akgöz, et al., Dynamic analysis of functionally graded porous microbeams under moving load, Transport in Porous Media, 142 (2022) 209–227.
[17] M. Davoodi Yekta, A. Rahi, Design of two layer clamped-clamped microsensor based on classical and non-classical theories, AUT Journal of Mechanical Engineering, 9(1) (2025) 19-32.
[18] A.C. Eringen, Microcontinuum field theories: I. Foundations and solids, Springer Science & Business Media, 2012.
[19] J. Peddieson, G.R. Buchanan, R.P. McNitt, Application of nonlocal continuum models to nanotechnology, International journal of engineering science, 41(3-5) (2003) 305-312.
[20] K. Kiani, H. Pakdaman, Bilaterally nonlocal dynamics of layer-by-layer assembly of double-walled carbon nanotubes accounting for intertube rigorous van der Waals forces, European Journal of Mechanics-A/Solids, 80 (2020) 103876.
[21] K. Kiani, H. Pakdaman, Nonlocal vibrations and potential instability of monolayers from double-walled carbon nanotubes subjected to temperature gradients, International Journal of Mechanical Sciences, 144 (2018) 576-599.
[22] H. Azimloo, G. Rezazadeh, R. Shabani, Bifurcation analysis of an electrostatically actuated nanobeam based on nonlocal theory considering centrifugal forces, International Journal of Nonlinear Sciences and Numerical Simulation, 21 (2020) 303–318.
[23] D.M. Tien, D.V. Thom, P.V. Minh, N.C. Tho, T.N. Doan, D.N. Mai, The application of the nonlocal theory and various shear strain theories for bending and free vibration analysis of organic nanoplates, Mechanics Based Design of Structures and Machines, 52(1) (2024) 588-610.
[24] K. Kiani, H. Pakdaman, Three-dimensional vibrations and instabilities of electron-transporting multi-layered graphene sheets via nonlocal-continuum-based models, Applied Mathematical Modelling, 145 (2025) 116103.
[25] Ö. Civalek, B. Uzun, M.Ö. Yayli, Torsional and longitudinal vibration analysis of a porous nanorod with arbitrary boundaries, Physica B: Condensed Matter, 633 (2022) 413761.
[26] H. Pakdaman, M. Roshan, S. Soltani, Vibrational analysis of two crossed graphene nanoribbons via nonlocal differential/integral models, Acta Mechanica, 235(2) (2024) 797-818.
[27] F. Khosravi, S.A. Hosseini, B.A. Hamidi, On torsional vibrations of triangular nanowire, Thin-Walled Structures, 148 (2020) 106591.
[28] S. Foroutan, A. Haghshenas, M. Hashemian, S.A. Eftekhari, D. Toghraie, Spatial buckling analysis of current-carrying nanowires in the presence of a longitudinal magnetic field accounting for both surface and nonlocal effects, Physica E: Low-dimensional Systems and Nanostructures, 97 (2018) 191-205.
[29] P. Lu, P. Zhang, H. Lee, C. Wang, J. Reddy, Non-local elastic plate theories, Proceedings of the Royal Society A: Mathematical, Physical and Engineering Sciences, 463(2088) (2007) 3225-3240.
[30] J. Phadikar, S. Pradhan, Variational formulation and finite element analysis for nonlocal elastic nanobeams and nanoplates, Computational materials science, 49(3) (2010) 492-499.
[31] Q.H. Pham, V.K. Tran, T.T. Tran, V.C. Nguyen, A.M. Zenkour, Nonlocal higher-order finite element modeling for vibration analysis of viscoelastic orthotropic nanoplates resting on variable viscoelastic foundation, Composite Structures, 318 (2023) 117067.
[32] R.A. Arpanahi, B. Mohammadi, M.T. Ahmadian, S.H. Hashemi, Study on the buckling behavior of nonlocal nanoplate submerged in viscous moving fluid, International Journal of Dynamics and Control, 11(6) (2023) 2820-2830.
[33] F. Ebrahimi, N. Shafiei, M. Kazemi, S.M. Mousavi Abdollahi, Thermo-mechanical vibration analysis of rotating nonlocal nanoplates applying generalized differential quadrature method, Mechanics of Advanced Materials and Structures, 24(15) (2017) 1257-1273.
[34] S. Dastjerdi, B. Akgöz, New static and dynamic analyses of macro and nano FGM plates using exact three-dimensional elasticity in thermal environment, Composite Structures, 192 (2018) 626-641.
[35] S. Chakraverty, L. Behera, Free vibration of rectangular nanoplates using Rayleigh–Ritz method, Physica E: Low-dimensional Systems and Nanostructures, 56 (2014) 357-363.
[36] H. Analooei, M. Azhari, A. Heidarpour, Elastic buckling and vibration analyses of orthotropic nanoplates using nonlocal continuum mechanics and spline finite strip method, Applied Mathematical Modelling, 37(10-11) (2013) 6703-6717.
[37] H. Tanzadeh, H. Amoushahi, Buckling analysis of orthotropic nanoplates based on nonlocal strain gradient theory using the higher-order finite strip method (H-FSM), European Journal of Mechanics-A/Solids, 95 (2022) 104622.

[38] S.S. Ma'en, W.G. Al-Kouz, Vibration analysis of non-uniform orthotropic Kirchhoff plates resting on elastic foundation based on nonlocal elasticity theory, International Journal of Mechanical Sciences, 114 (2016) 1-11.
[39] Y. Zhang, L. Zhang, K. Liew, J. Yu, Buckling analysis of graphene sheets embedded in an elastic medium based on the kp-Ritz method and non-local elasticity theory, Engineering Analysis with Boundary Elements, 70 (2016) 31-39.
[40] Ö. Civalek, B. Akgöz, Vibration analysis of micro-scaled sector shaped graphene surrounded by an elastic matrix, Computational Materials Science, 77 (2013) 295-303.
[41] S.H. Hashemi, H. Mehrabani, A. Ahmadi-Savadkoohi, Forced vibration of nanoplate on viscoelastic substrate with consideration of structural damping: An analytical solution, Composite Structures, 133 (2015) 8-15.
[42] S. Pradhan, J. Phadikar, Nonlocal elasticity theory for vibration of nanoplates, Journal of Sound and Vibration, 325(1-2) (2009) 206-223.
[43] M. Panyatong, B. Chinnaboon, S. Chucheepsakul, Free vibration analysis of FG nanoplates embedded in elastic medium based on second-order shear deformation plate theory and nonlocal elasticity, Composite Structures, 153 (2016) 428-441.
[44] R. Aghababaei, J. Reddy, Nonlocal third-order shear deformation plate theory with application to bending and vibration of plates, Journal of Sound and Vibration, 326(1-2) (2009) 277-289.
[45] M. Ilkhani, A. Bahrami, S. Hosseini-Hashemi, Free vibrations of thin rectangular nano-plates using wave propagation approach, Applied Mathematical Modelling, 40(2) (2016) 1287-1299.
[46] D. Rong, J. Fan, C. Lim, X. Xu, Z. Zhou, A new analytical approach for free vibration, buckling and forced vibration of rectangular nanoplates based on nonlocal elasticity theory, International Journal of Structural Stability and Dynamics, 18(04) (2018) 1850055.
[47] S. Hosseini-Hashemi, M. Zare, R. Nazemnezhad, An exact analytical approach for free vibration of Mindlin rectangular nano-plates via nonlocal elasticity, Composite Structures, 100 (2013) 290-299.
[48] S. Hosseini-Hashemi, M. Kermajani, R. Nazemnezhad, An analytical study on the buckling and free vibration of rectangular nanoplates using nonlocal third-order shear deformation plate theory, European Journal of Mechanics-A/Solids, 51 (2015) 29-43.
[49] X. Zheng, M. Huang, D. An, C. Zhou, R. Li, New analytic bending, buckling, and free vibration solutions of rectangular nanoplates by the symplectic superposition method, Scientific Reports, 11(1) (2021) 2939.
[50] Z. Wang, Y. Xing, Q. Sun, Y. Yang, Highly accurate closed-form solutions for free vibration and eigenbuckling of rectangular nanoplates, Composite Structures, 210 (2019) 822-830.
[51] Z. Qin, S. Zhao, X. Pang, B. Safaei, F. Chu, A unified solution for vibration analysis of laminated functionally graded shallow shells reinforced by graphene with general boundary conditions, International Journal of Mechanical Sciences, 170 (2020) 105341.
[52] G. Jin, X. Ma, S. Shi, T. Ye, Z. Liu, A modified Fourier series solution for vibration analysis of truncated conical shells with general boundary conditions, Applied Acoustics, 85 (2014) 82-96.
[53] D. Zhou, Y. Cheung, F. Au, S. Lo, Three-dimensional vibration analysis of thick rectangular plates using Chebyshev polynomial and Ritz method, International Journal of Solids and Structures, 39(26) (2002) 6339-6353.
[54] H. Lin, D. Cao, A unified Gram-Schmidt-Ritz formulation for vibration and active flutter control analysis of honeycomb sandwich plate with general elastic support, Journal of Vibroengineering, 20(5) (2018) 1982-2000.
[55] Z. Qin, F. Chu, J. Zu, Free vibrations of cylindrical shells with arbitrary boundary conditions: a comparison study, International Journal of Mechanical Sciences, 133 (2017) 91-99.
[56] S. Zhao, X. Zhang, S. Zhang, B. Safaei, Z. Qin, F. Chu, A unified modeling approach for rotating flexible shaft-disk systems with general boundary and coupling conditions, International Journal of Mechanical Sciences, 218 (2022) 107073.
[57] B. Qin, R. Zhong, Q. Wu, T. Wang, Q. Wang, A unified formulation for free vibration of laminated plate through Jacobi-Ritz method, Thin-Walled Structures, 144 (2019) 106354.
[58] X. Song, G. Jin, T. Ye, S. Zhong, A formulation for turbulent-flow-induced vibration of elastic plates with general boundary conditions, International Journal of Mechanical Sciences, 205 (2021) 106602.
[59] G. Li, Y. Xing, Z. Wang, Closed-form solutions for free vibration of rectangular nonlocal Mindlin plates with arbitrary homogeneous boundary conditions, Composites Part C: Open Access, 6 (2021) 100193.
[60] C. Li, S.K. Lai, X. Yang, On the nano-structural dependence of nonlocal dynamics and its relationship to the upper limit of nonlocal scale parameter, Applied Mathematical Modelling, 69 (2019) 127-141.
[61] C.L. Dym, I.H. Shames, Solid mechanics, Springer, 1973.
[62] Y. Song, K. Xue, Q. Li, A solution method for free vibration of intact and cracked polygonal thin plates using the Ritz method and Jacobi polynomials, Journal of Sound and Vibration, 519 (2022) 116578.

[63] R.B. Bhat, Natural frequencies of rectangular plates using characteristic orthogonal polynomials in Rayleigh-Ritz method, Journal of sound and vibration, 102(4) (1985) 493-499.
[64] Y. Liang, Q. Han, Prediction of the nonlocal scaling parameter for graphene sheet, European Journal of Mechanics-A/Solids, 45 (2014) 153-160.
[65] S. Sahmani, A. M. Fattahi, Calibration of developed nonlocal anisotropic shear deformable plate model for uniaxial instability of 3D metallic carbon nanosheets using MD simulations, Computer Methods in Applied Mechanics and Engineering, 322 (2017) 187-207.
[66] M. Shariati, S. S. M. N. Souq, B. Azizi, Surface- and nonlocality-dependent vibrational behavior of graphene using atomistic-modal analysis, International Journal of Mechanical Sciences, 228 (2022) 107471.
[67] S. H. Madani, M. H. Sabour, M. Fadaee, Molecular dynamics simulation of vibrational behavior of annular graphene sheet: Identification of nonlocal parameter, Journal of Molecular Graphics and Modelling, 79 (2018) 264-272.